JCI insight

RESEARCH ARTICLE

CD8+ T cells in beige adipogenesis and energy homeostasis

Maria Moysidou,[1,2] Sevasti Karaliota,[1] Elisavet Kodela,[1,2] Maria Salagianni,[1] Yassemi Koutmani,[1] Antonia Katsouda,[1] Konstantia Kodella,[1] Panagiotis Tsakanikas,[1] Styliani Ourailidou,[1] Evangelos Andreakos,[1] Nikolaos Kostomitsopoulos,[1] Dimitris Skokos,[3] Antonios Chatzigeorgiou,[4] Kyoung-Jin Chung,[4] Stefan Bornstein,[4] Mark W. Sleeman,[5] Triantafyllos Chavakis,[4] and Katia P. Karalis[1,4,6]

[1]Clinical, Experimental Surgery & Translational Research, Biomedical Research Foundation Academy of Athens, Athens, Greece. [2]University of Crete, School of Medicine, Heraklion, Crete, Greece. [3]Regeneron Pharmaceuticals Inc., Tarrytown, New York, USA. [4]Technische Universität Dresden, School of Medicine, Dresden, Germany. [5]Department of Physiology, Monash University, Clayton, Victoria, Australia. [6]Endocrine Division, Boston Children's Hospital, Boston, Massachusetts, USA.

Although accumulation of lymphocytes in the white adipose tissue (WAT) in obesity is linked to insulin resistance, it remains unclear whether lymphocytes also participate in the regulation of energy homeostasis in the WAT. Here, we demonstrate enhanced energy dissipation in Rag1$^{-/-}$ mice, increased catecholaminergic input to subcutaneous WAT, and significant beige adipogenesis. Adoptive transfer experiments demonstrated that CD8$^+$ T cell deficiency accounts for the enhanced beige adipogenesis in Rag1$^{-/-}$ mice. Consistently, we identified that CD8$^{-/-}$ mice also presented with enhanced beige adipogenesis. The inhibitory effect of CD8$^+$ T cells on beige adipogenesis was reversed by blockade of IFN-γ. All together, our findings identify an effect of CD8$^+$ T cells in regulating energy dissipation in lean WAT, mediated by IFN-γ modulation of the abundance of resident immune cells and of local catecholaminergic activity. Our results provide a plausible explanation for the clinical signs of metabolic dysfunction in diseases characterized by altered CD8$^+$ T cell abundance and suggest targeting of CD8$^+$ T cells as a promising therapeutic approach for obesity and other diseases with altered energy homeostasis.

Introduction

Obesity, a major epidemic with prevalence rates rising steadily among adults and children worldwide, is characterized by excessive accumulation of white adipose tissue (WAT). Obesity is normally associated with the development of a low-grade inflammatory response within WAT, attributed initially to the infiltration of macrophages in the adipose tissue as well as a shift in macrophage polarization (1). Additionally, further cells of innate and adaptive immunity, such as mast cells (2), eosinophils (3), neutrophils (4), type 2 innate lymphoid cells (ILC2s) (5), and CD4$^+$ (6) and CD8$^+$ T cells (7) as well as Tregs (8, 9), have been implicated as either positive or negative regulators of adipose tissue function and of insulin resistance. A major feature of the adipose tissue is its inherent capacity to act as an energy storage and/or energy dissipation site (10). This dual function has been linked to the distinct WAT and brown adipose tissue (BAT) depots respectively, and the high expression of the mitochondrial uncoupling protein 1 (Ucp1) in the latter (11, 12). A series of recent studies identified multilocular cells with energy-dispensing activity, named "beige" adipocytes (13–16), within the subcutaneous WAT (scWAT). Beige adipocytes may derive either from PDGFRα$^+$, Sca1$^+$, and CD34$^+$ precursor cells (17) or via transdifferentiation of white adipocytes (18, 19). Beige adipocytes (15, 16), similar to the brown adipocytes, express Ucp1, are expanded in response to challenges such as cold exposure, and, when activated, increase fatty acid oxidation (20). Recent findings indicate that, in adult humans, what has been thought as brown fat is more likely formed by beige, rather than brown, adipocytes (16), confirming the significance of beige adipose depot in adulthood. As shown, induction of adipose tissue thermogenesis and/or browning of white fat promote efficient whole-body energy expenditure (21). Emerging evidence suggests novel roles for innate immune cells in regulating energy dissipation via the scWAT (22–24). More importantly, increased numbers of ILC2s in the scWAT have been shown to promote beiging by stimulating the proliferation of PDGFRα$^+$ progenitors via secretion of the interleukins IL-5 and -13 (17). Eosinophils have

Authorship note: MM and SK are co–first authors.

Conflict of interest: The authors have declared that no conflict of interest exists.

Submitted: May 31, 2017
Accepted: February 1, 2018
Published: March 8, 2018

Reference information:
JCI Insight. 2018;3(5):e95456.
https://doi.org/10.1172/jci.insight.95456.

been shown to interact with M2-like macrophages in promoting beige adipogenesis as well (22, 24), while M1 macrophages inhibit scWAT beiging in obesity (25, 26). On the contrary, nothing has been reported so far about a function of lymphocytes on beige adipogenesis, which is the subject of the present work.

In this study, we demonstrate increased beige adipogenesis in the scWAT of Rag1$^{-/-}$ lymphocyte-deficient mice accompanied by increased efficiency in lipid utilization in their WAT depots. We also show that the major immune cell type driving the development of this phenotype is the CD8$^+$ T cell. We provide evidence that CD8$^+$ T cells can modify the catecholaminergic activity of WAT and affect the number of ILCs and eosinophils as well as the cytokines involved in regulating their functions. Our findings suggest that these effects of the CD8$^+$ T cells are mediated via secreted factors and, particularly, IFN-γ. Overall, our study highlights the important role of lymphocytes in the regulation of beige adipose tissue formation via direct interaction with cells of innate immunity and modulation of the catecholaminergic activity.

Results

Lymphocyte deficiency induces beige adipogenesis. Given the emerging evidence on the role of immune cells in the regulation of metabolism, we first assessed the potential effects of lymphocyte deficiency in systemic metabolic activity. To this end, we performed indirect calorimetry in age- and weight-matched Rag1$^{-/-}$ and WT male mice, using a comprehensive laboratory animal monitoring system (CLAMS). To our surprise, Rag1$^{-/-}$ mice dissipated more energy than WT mice, despite their similar eating and motor behaviors (Figure 1, A–C, and Supplemental Figure 1, A–C; supplemental material available online with this article; https://doi.org/10.1172/jci.insight.95456DS1). Additionally, the respiratory exchange ratio (RER) was found to be lower in Rag1$^{-/-}$ mice (Figure 1D and Supplemental Figure 1D), which was suggestive of an increased utilization of fatty acids as their energy substrate. In agreement, the epididymal WAT (epiWAT) was of lower weight in Rag1$^{-/-}$ mice (Supplemental Figure 1, E and F). Further, gene expression profiling revealed a significant shift in the expression of factors involved in lipid catabolism in the Rag1$^{-/-}$ epiWAT, indicating the impact of lymphocyte deficiency in the regulation of this process (Supplemental Figure 1G).

The increased energy expenditure that has been identified in the Rag1$^{-/-}$ mice raised the possibility for associated enhancement of brown and/or beige adipogenesis. Even though we found no differences between the Rag1$^{-/-}$ and WT BAT, as per weight, H&E analysis, or Ucp1 expression (Supplemental Figure 1, H–J), H&E staining of the scWAT identified substantially increased abundance of beige adipose tissue in Rag1$^{-/-}$, as compared with WT, biopsies (Figure 1E). In agreement, the expression of genes associated with beige adipogenesis, such as Ucp1, cell death–inducing DFFA-like effector a (Cidea), PR domain-containing 16 (Prdm16), and Fgf21 (Figure 1F) (13, 27), was significantly induced in the Rag1$^{-/-}$ scWAT. Finally, the weight of the Rag1$^{-/-}$ scWAT was significantly lower, in accordance with its higher content in small, energy-dissipating, rather than in large, primarily lipid-storing, adipocytes (Figure 1G). These findings suggest that lymphocyte deficiency promotes energy dissipation by inducing beige adipogenesis in the lipid-storing WAT, while it has no apparent effect on BAT, the primary thermogenic depot (12). A mechanistic insight on the increased formation of beige adipose tissue in the Rag1$^{-/-}$ mice was provided by the increased expression of the gene encoding the adrenergic receptor (AdR) 1α (AdR1α) and a similar trend for the AdRβ3 gene in the Rag1$^{-/-}$ scWAT (Figure 1F). Further, treatment of Rag1$^{-/-}$ mice with the selective α-1 AdR antagonist prazosin hydrochloride via the drinking water for 5 days led to reduced amounts of beige adipose tissue (Supplemental Figure 1K) and significant attenuation in the corresponding expression of Ucp1 and Prdm16 (Supplemental Figure 1L). Taken together, these results indicate that the increased beige adipogenesis in Rag1$^{-/-}$ mice is associated with induction of adrenergic activity, a physiologically relevant pathway, in the WAT depot (14).

To further confirm the specificity of the Rag1$^{-/-}$ scWAT phenotype, we repeated the experiment at thermoneutrality, i.e., at a housing temperature of 30°C (28). Following housing of all groups at thermoneutrality conditions for 20 days, Ucp1 expression decreased significantly in both WT and Rag1$^{-/-}$ mice (Figure 1H), as expected by the well-shown sensitivity of this factor to temperature changes (28–30). No differences in the weight of the scWAT were found between the two genotypes when housed in thermoneutrality conditions (data not shown). However, in Rag1$^{-/-}$ scWAT genes associated with beige adipogenesis, such as Cidea, were found to be at significantly higher levels as compared with the WT scWAT (Figure 1H). The latter is in line with the corresponding histological analysis that showed profound abundance of beige fat areas in the scWAT of the Rag1$^{-/-}$ mice (Figure 1I).

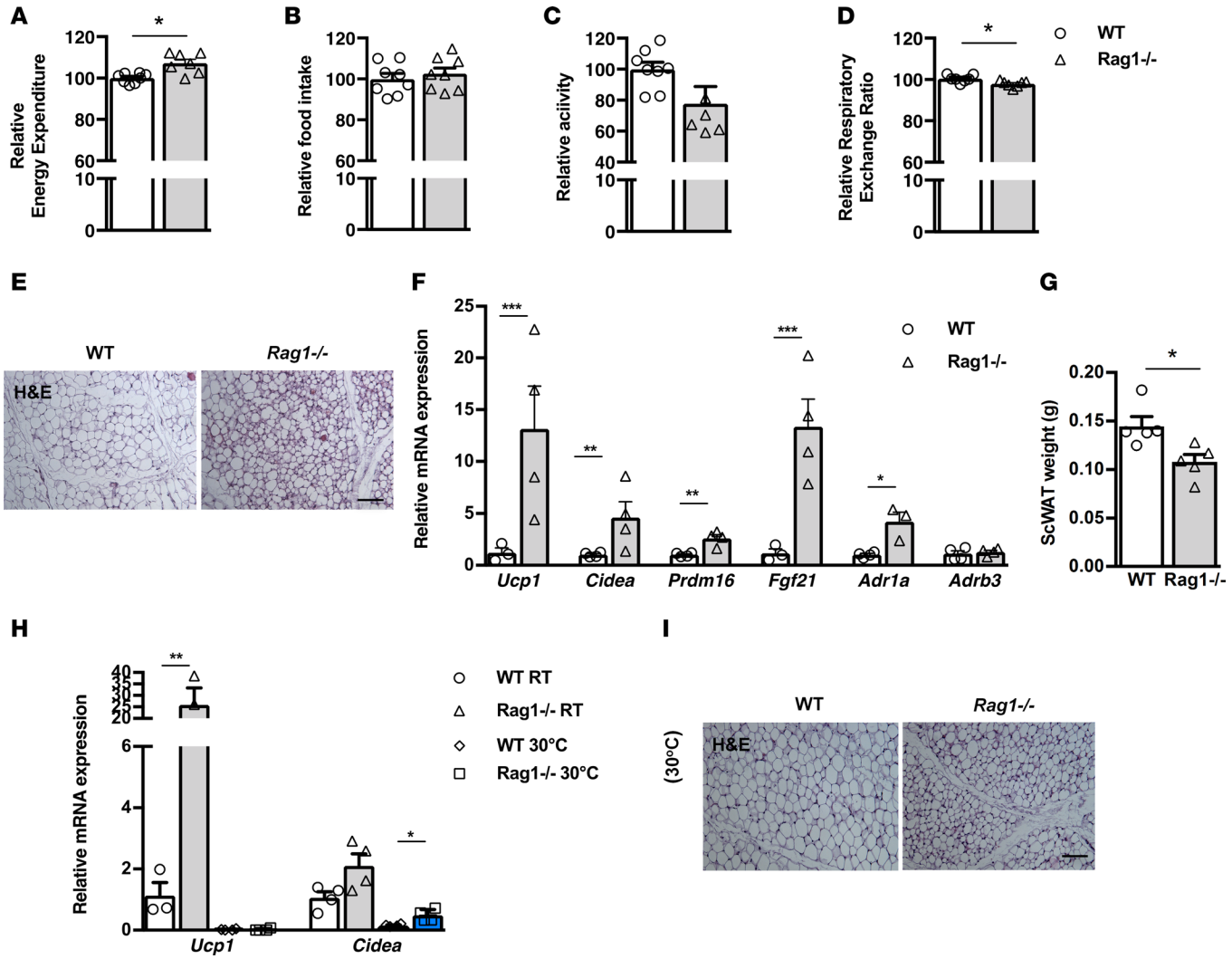

Figure 1. Beige tissue formation in the scWAT is increased in lymphocyte-deficient mice. (**A–D**) Assessment of metabolic behavior using indirect calorimetry, including energy expenditure adjusted to body weight (**A**), food intake (**B**), total activity (**C**), and respiratory exchange ratio (RER) (**D**). $n = 7$ per group. (**E**) Representative H&E-stained images of the scWAT depot of age- and weight-matched Rag1$^{-/-}$ and WT mice. Scale bar: 100 μm. (**F**) Gene expression analysis of thermogenic and adrenergic receptors. Data are shown as mean expression normalized to actin ± SEM. (**G**) Absolute weight of scWAT in age- and weight-matched WT and Rag1$^{-/-}$ mice. The data shown are derived from 1 representative of 3 independent experiments. (**H**) Gene expression analysis of Ucp1 and Cidea in WT and Rag1$^{-/-}$ mice to assess the effect of thermoneutrality, simulated by housing at 30°C for 20 days. Data are shown as mean expression normalized to actin ± SEM. (**I**) Representative H&E-stained images in the above groups. Scale bar: 100 μm. Data shown are derived from 1 representative of 2 independent experiments. Data are presented as mean ± SEM. $n \geq 4$ per group (**E–I**). *$P < 0.05$, **$P < 0.01$, ***$P < 0.001$, Student's t test.

Next, we sought to confirm that lymphocyte deficiency is indeed the primary underlying reason for the enhanced beige adipogenesis in Rag1$^{-/-}$ mice by reconstituting mice with splenocytes isolated from WT mice. This procedure reversed the phenotype of the Rag1$^{-/-}$ scWAT, as it resulted in significant elimination of the extent of the beige fat areas, resembling those found in the WT scWAT (Figure 2, A and B). Splenocyte reconstitution also led to increased adipocyte size (Figure 2C), an additional indication for the increase in energy storage, while it reduced the expression of thermogenic and lipid oxidation-related genes to levels comparable to those in the WT tissues (Figure 2D). The weight of WT scWAT was not altered, compared with the Rag1$^{-/-}$ tissue, following reconstitution with splenocytes (data not shown). Further, reconstitution of the Rag1$^{-/-}$ mice with splenocytes reduced the expression of TH, the rate-limiting step in catecholamine synthesis (Figure 2A) and of the AdR1α and AdRβ3 genes (Figure 2D). These data provide additional evidence for the link between lymphocyte deficiency and increased adrenergic activation.

CD8$^+$ T cell transfer abrogates beige adipogenesis in Rag1$^{-/-}$ mice. Next, we sought to identify the specific lymphocyte population missing in the Rag1$^{-/-}$ mice, possibly underlying the induction in their beige adi-

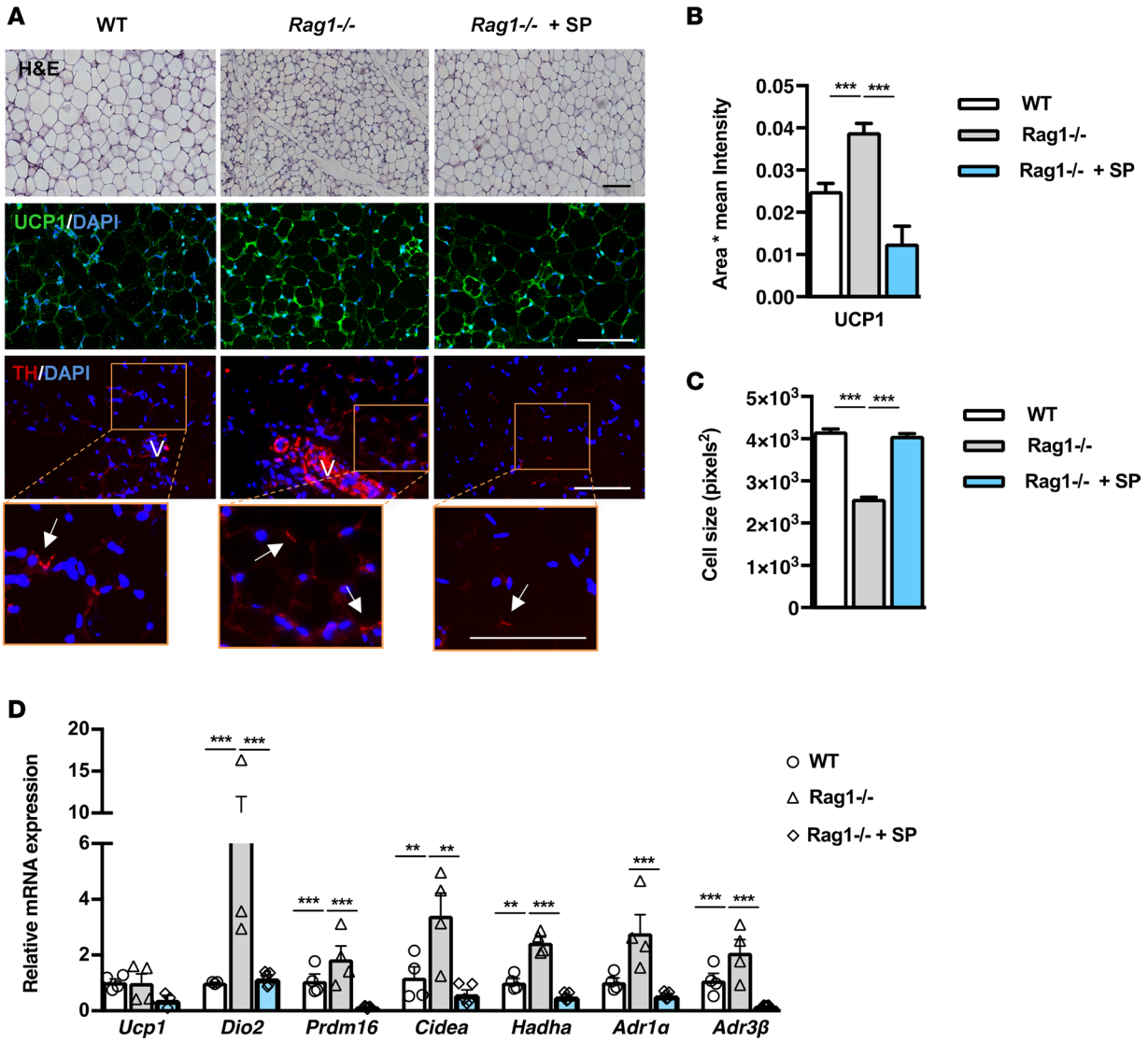

Figure 2. Adoptive transfer of whole splenocytes in Rag1$^{-/-}$ mice reverses the increased scWAT beiging. (**A**) Representative images of H&E and immunofluorescence (IF) staining for UCP1 or TH from WT, Rag1$^{-/-}$, or Rag1$^{-/-}$ mice reconstituted with 5×10^6 splenocytes, once a week for 2 weeks. Arrows represent the TH$^+$cells. V represents the vessels. Scale bar: 100 μm. (**B**) The relative UCP1 mean area and intensity in the above groups. Values represent the mean ± SD intensity of 15 patches for every image. $n = 3$ per group. (**C**) Relative scWAT adipocyte cell size of WT mice or Rag1$^{-/-}$ mice treated with PBS or adoptively transferred with splenocytes (5×10^6), once a week for 2 weeks. $n = 4$ per group. (**D**) Relative expression of beige, oxidation, and adrenergic receptors genes. Data are shown as mean expression normalized to actin ± SEM. $n = 5$ per group. Data are representative of 1 of 2 separate experiments. Data are presented as mean ± SEM. $^{**}P < 0.01$, $^{***}P < 0.001$. 1-way ANOVA with Bonferroni's post test.

pogenesis. Previous studies have described the contribution of the resident and/or infiltrated lymphocyte populations, including CD4$^+$ and CD8$^+$ T cells, to WAT biology (6, 7, 31). In particular, the CD8$^+$ T cells have been directly associated with lipid metabolism, as shown by their striking effects in promoting liver steatosis (32). We therefore assessed the effect of reconstitution of the Rag1$^{-/-}$ mice with CD8$^+$ T cells, on the beiging of their scWAT. CD8$^+$ T cells isolated from WT mouse splenocytes were transferred into Rag1$^{-/-}$ mice by retro-orbital administration. There was no difference in the weight of the scWAT between control Rag1$^{-/-}$ mice and those reconstituted with CD8$^+$ T cells (data not shown), while as expected, the abundance of CD8$^+$ T cells was substantially increased in the reconstituted scWAT (Supplemental Figure 2A). In line with the hypothesis attributing the increased beiging of the Rag1$^{-/-}$ scWAT to their lymphocyte deficiency, the reconstituted scWAT was characterized by attenuated beiging (Figure 3A). In line with this, reconstituted scWAT showed significantly compromised expression of AdR1α and AdRβ3 and of genes encoding proteins involved in thermogenesis, such as Ucp1, Cidea, Fgf21, and in lipid catabolism, such as Hadha and Lipe (Figure 3B). Upon reconstitution with CD8$^+$ T cells, the expression of UCP1 protein, the main protein

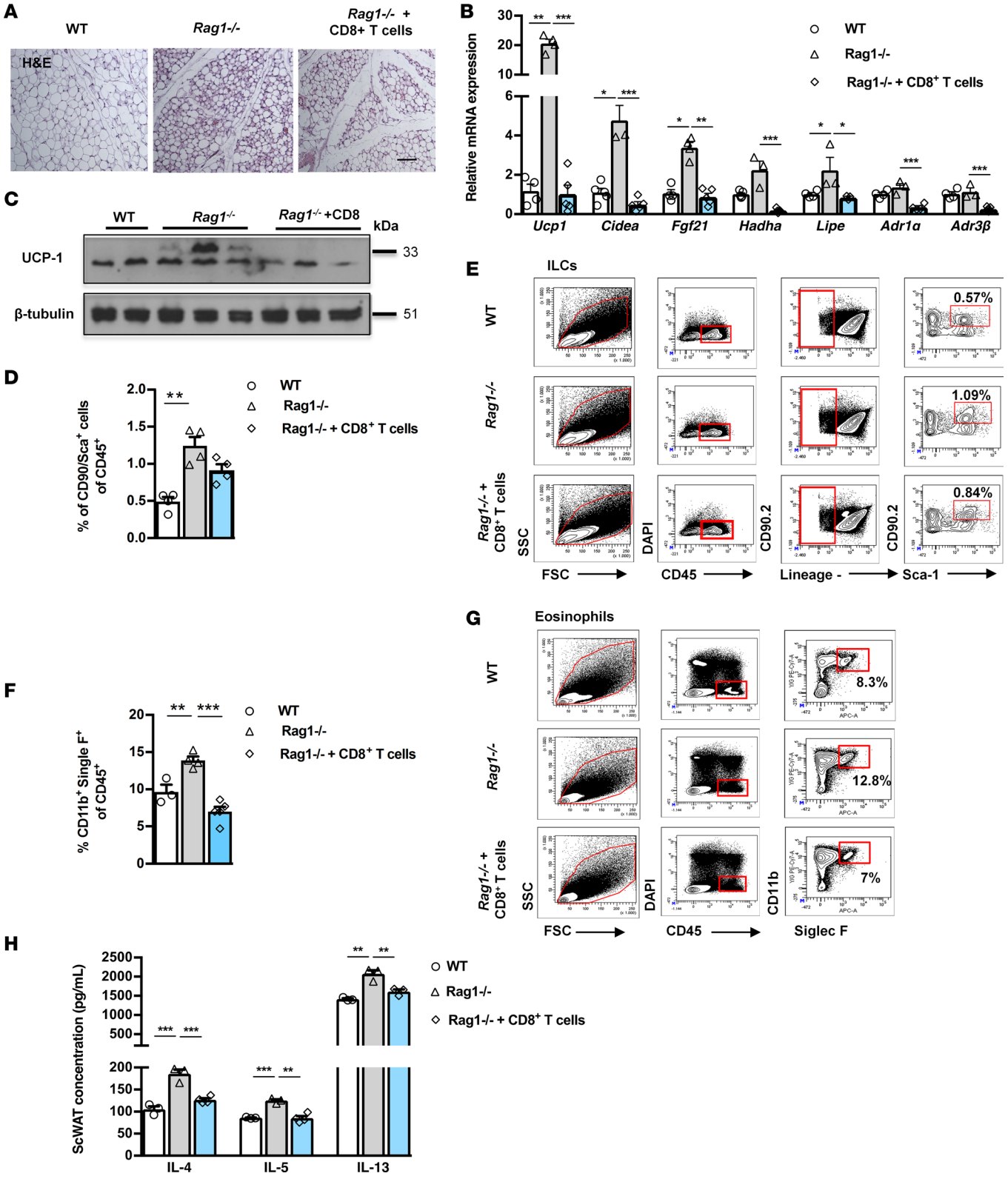

Figure 3. Adoptive transfer of CD8⁺ T cells in Rag1$^{-/-}$ mice reverses increased scWAT beiging in Rag1$^{-/-}$ mice and decreases ILCs and eosinophils. Data shown are from the scWAT of WT, Rag1$^{-/-}$, or Rag1$^{-/-}$ mice reconstituted with 5 × 10^6 CD8⁺ T cells, once a week for 2 weeks. (**A**) Representative H&E staining. Scale bar: 100 μm. n = 3 per group. (**B**) Expression of thermogenic, lipid metabolism, and adrenergic receptors genes. Data are shown as mean expression normalized to actin ± SEM. $n \geq 5$. Data shown are derived from 1 representative of 3 independent experiments (**C**) Protein expression of UCP1 and β-tubulin. (**D**) Percentage of ILCs (CD90.2⁺Sca-1⁺Lin⁻) gated on CD45⁺ cells. $n \geq 4$ per group. (**E**) Representative gating strategy for the identification of ILCs (CD90.2⁺ Sca-1⁺ Lin⁻). Percentage of CD90.2⁺Sca-1⁺Lin⁻ gated on the viable CD45⁺DAPI⁻ cells. Data shown are representative of 2 independent experiments. Flow cytometry was performed after pooling $n \geq 5$ mice per group. (**F**) Percentage of eosinophils gated (CD11b⁺Siglec F⁺) on the viable CD45⁺DAPI⁻ cells. $n \geq 4$ per group. (**G**) Representative gating strategy for identification of eosinophils (CD11b⁺Siglec F⁺). Percentage

of CD11b$^+$Siglec F$^+$ cells gated on the viable CD45$^+$DAPI$^-$ cells. Data shown are representative of 2 independent experiments. Flow cytometry was performed after pooling $n \geq 5$ mice per group. (**H**) Intra-scWAT levels of IL-4, IL-5, and IL-13. $n \geq 4$ per group. Data are presented as mean ± SEM. $^*P < 0.05$, $^{**}P < 0.01$, $^{***}P < 0.001$, 1-way ANOVA with Bonferroni's post test.

associated with beige adipogenesis, was dramatically reduced in the Rag1$^{-/-}$ scWAT (Figure 3C). The above findings argue for CD8$^+$ T cell deficiency as the potential driving mechanism behind the induction of energy dissipation in the Rag1$^{-/-}$ WAT.

Interaction between scWAT CD8$^+$ T cells and cells of innate immunity. As has been demonstrated in a number of studies, the relative abundance and the polarization of macrophages are both important determinants for the development of insulin resistance and the associated inflammatory features of obesity. The majority of adipose tissue macrophages in baseline conditions bear characteristics of "alternatively activated M2-like cells," while as obesity develops, "M1-like" proinflammatory macrophages become the predominant population (1). We detected no major differences in either the percentages or absolute numbers of CD11b$^+$ F4/80$^+$ cells expressed per gram of tissue of the scWAT between WT and Rag1$^{-/-}$ mice with or without reconstitution with CD8$^+$ T cells (Supplemental Figure 2, B and C). Further, we found no evidence for altered macrophage polarization in either of the experimental groups based on assessment of M1 and M2 markers (Supplemental Figure 2D). These data suggest that a shift or polarization in the scWAT macrophage content is unlikely to mediate the effects of lymphocyte deficiency on beige adipogenesis.

Emerging evidence demonstrates the specific contribution of particular components of type 2 immunity, like ILC2s and eosinophils, in the regulation of beige adipogenesis (3, 5). We sought to assess the potential link between these studies and our current findings by assessment of the effect of lymphocyte deficiency on the abundance of eosinophils and ILCs in the scWAT of WT, Rag1$^{-/-}$, and Rag1$^{-/-}$ mice reconstituted with CD8$^+$ T cells. Specifically, ILCs were defined as CD45$^+$, lineage$^-$ (CD3$^-$CD4$^-$CD8$^-$CD19$^-$B220$^-$ CD11b$^-$CD11c$^-$FceRI$^-$Gr-1$^-$Terr119$^-$), CD90.2$^+$Sca-1$^+$ cells. We found that the percentage of CD90$^+$Sca-1$^+$ cells gated on CD45$^+$ cells in Rag1$^{-/-}$ scWAT was significantly higher (1.244% ± 0.117%) than that of the WT scWAT (0.491% ± 0.061%) (Figure 3, D and E). Accordingly, the absolute numbers of ILCs (CD90.2$^+$Sca-1$^+$) per gram of tissue in the Rag1$^{-/-}$ scWAT were also significantly increased (Supplemental Figure 2E). A similar pattern was obtained in eosinophils, defined as CD45$^+$CD11b$^+$Siglec F$^+$ cells. Specifically, the percentage of eosinophils gated on CD45$^+$ cells (Figure 3, F and G) was higher in Rag1$^{-/-}$ scWAT (WT: 9.667% ± 0.953%; Rag1$^{-/-}$: 13.900% ± 0.521%), although the absolute numbers of eosinophils did not reach significantly different levels between the two genotypes (Supplemental Figure 2F).

Reconstitution of Rag1$^{-/-}$ mice with CD8$^+$ T cells reversed the expanded ILC (0.912% ± 0.081%) and eosinophil (7.000% ± 0.646%) populations to levels comparable to those detected in the WT scWAT (Figure 3, D–G, and Supplemental Figure 2, D and E). These findings indicate the dynamic relation between CD8$^+$ T and the cells of the innate immune system, further highlighted by the associated cytokines levels, such as IL-4 or IL-5 and IL-13, measured in the scWAT of the aforementioned experimental groups (Figure 3H). Along these lines, a recent report showed that the IL-33–induced ILC2s regulate energy homeostasis by increasing the energy expenditure via induction of beige adipogenesis (33), shown to be mediated by the intra-scWAT levels of IL-4, -5, and -13 (24, 33–35). Together, our findings provide evidence that in Rag1$^{-/-}$ scWAT enhanced activation of innate cells due to lack of CD8$^+$ T cells may account for their enhanced beige adipogenesis.

CD8$^+$ T cells block cold exposure–induced beige adipogenesis. Next, we asked if Rag1$^{-/-}$ mice retain their ability to respond to stimuli driving the beiging of scWAT, despite their already substantially expanded beige depot at baseline conditions (Figure 1). For this purpose, we exposed WT and Rag1$^{-/-}$ mice to cold via housing at 4°C, for a period of 2 days (16, 36). We found that Rag1$^{-/-}$ mice could adapt better to cold and thus resisted hypothermia more efficiently than WT mice, as depicted by the profiling of core body temperature over time (Figure 4A), while there were no differences between the WT and Rag1$^{-/-}$ scWAT weights (data not shown). Maintenance of homeostasis upon cold exposure is achieved by catecholamine-induced thermogenesis (16). Tyrosine hydroxylase (TH), the rate-limiting step in the biosynthesis of norepinephrine (37, 38) and a reliable routinely used marker for catecholaminergic neurons (19), was higher in the Rag1$^{-/-}$ scWAT upon exposure to cold (Figure 4B). We confirmed, by double immunofluorescent staining for TH and for the neuronal marker class III β-tubulin (Tuj1), that TH$^+$ cells in the scWAT are neuronal cells (39–43) by costaining with TH and the neuronal marker, Tuj1, of control (WT) scWAT sections (Supplemental Figure 3A). As expected, cold exposure led to significant induction of scWAT beiging and of corresponding Ucp1 expression in

both WT and Rag1$^{-/-}$ mice (Figure 4, B and C). The differences in the expression of other scWAT genes between WT and Rag1$^{-/-}$ mice were not as prominent as those detected in room temperature conditions (Figure 4C). Most importantly, the expression of UCP1 protein (Figure 4B and Supplemental Figure 3B) and TH remained substantially higher in the Rag1$^{-/-}$ scWAT (Figure 4B), highlighting the contribution of the lymphocyte deficiency to beige adipogenesis, even in states associated with excess beige fat development. All the above indicate that Rag1$^{-/-}$ mice retain their ability to respond to physiological challenges, such as cold, that drive beige adipogenesis, despite their constitutively increased beige adipogenesis.

The better adaptation of the Rag1$^{-/-}$ mice to cold exposure was attenuated by reconstitution with CD8^{+} T cells. Furthermore, this intervention reduced beige adipogenesis and decreased the expression of TH and the associated AdRs (Figure 4, A–C) in the scWAT of the Rag1$^{-/-}$ mice. However, the scWAT weight of reconstituted mice was not different compared with Rag1$^{-/-}$ mice (data not shown).

Next, we assessed the effect of cold exposure on the abundance of eosinophils and ILCs in the scWAT. Consistent with the above results, reconstitution of Rag1$^{-/-}$ mice with CD8^{+} T cells led to a significant reduction in the percentage of both eosinophils (11.150% ± 0.902%) and ILCs (1.265% ± 0.065%) gated on CD45^{+} cells, compared with those of the nontreated Rag1$^{-/-}$ mice (eosinophils: 17.150% ± 2.293%; ILCs:1.759% ± 0.189%) (Figure 4, D–G), while their absolute numbers did not display any significant difference (data not shown). At the same time, both eosinophils and ILCs were significantly higher in the cold-exposed Rag1$^{-/-}$ mice as compared with WT mice (eosinophils: 6.800% ± 2.491%; ILCs: 0.943% ± 0.044%) (Figure 4, D and F). This finding indicates that both eosinophils and the total ILCs may participate in the cold-induced beiging of Rag1$^{-/-}$ mice. The absolute numbers of eosinophils (WT: 34,082.84; Rag1$^{-/-}$: 35,087.72) and ILCs (WT: 3,393,272.00; Rag1$^{-/-}$: 3,810,893.00) per gram of tissue are relatively higher in Rag1$^{-/-}$ mice compared with WT mice.

CD8^{+} T cells, the main lymphocytes regulating beige adipogenesis. To strengthen our hypothesis that the absence of CD8^{+} T cells in Rag1$^{-/-}$ mice accounted for the increased beiging in their scWAT, we compared the phenotype of the scWAT in CD8^{+} T cell–deficient (CD8$^{-/-}$) and WT mice. Initially, we performed indirect calorimetry in age- and weight-matched CD8$^{-/-}$ and WT mice using CLAMS, and we found increased expenditure of energy in the CD8$^{-/-}$ mice compared with the WT mice (Figure 5A). This could be explained by the fact that CD8$^{-/-}$ mice showed increased total activity (Figure 5B), while they consumed the same amount of food as the WT mice (Figure 5C). Additionally, RER was found to be lower in the CD8$^{-/-}$ mice, suggesting that, in the absence of CD8^{+} T cells, mice shift to preferential usage of fatty acids, rather than carbohydrates, as energy substrate (Figure 5D). In line with their metabolic profile, we found that CD8$^{-/-}$ mice exhibited a significant expansion of the beige fat areas in scWAT; increased expression of beige-driving genes, such as Ucp1, Cidea, and Dio2 (Figure 5, E and F); and higher percentage of eosinophils content (Figure 5G) compared with the WT mice. However, we found no apparent differences between the scWAT and BAT weights between the two genotypes, despite the increase in the epiWAT weight in the CD8$^{-/-}$ mice (Supplemental Figure 4A), a finding of unknown significance as of now. We confirmed the above with complementary studies in WT mice treated either with anti-CD8 antibody or control IgG that supported the impact of CD8^{+} T cell depletion in the development of beige fat (Supplemental Figure 4B). Further, exposure to cold environment resulted in the anticipated activation of beige adipogenesis (Figure 5, H and I) and the associated increase in eosinophils in scWAT (Figure 5J). The absolute number of eosinophils per gram of tissue was 1,285,714 in CD8$^{-/-}$ mice versus 842,105 in WT mice. No changes were detected in the scWAT weights of age- and weight-matched WT and CD8$^{-/-}$ mice following cold exposure (data not shown).

IFN-γ negatively regulates beige adipogenesis. To further elucidate the specific factor(s) underlying the effects of CD8^{+} T cells in beige adipogenesis, we next measured the scWAT content in IFN-γ, a cytokine secreted in large amounts by activated CD8^{+} T cells and implicated in the regulation of resident innate immune cells within the scWAT (39, 40). Intra-scWAT IFN-γ showed a tendency to decrease levels in the Rag1$^{-/-}$ tissue; this difference was, however, abolished following reconstitution with CD8^{+} T cells (Supplemental Figure 5A). To confirm the specific role of CD8-derived IFN-γ in this process, we reconstituted Rag1$^{-/-}$ mice with CD8^{+} T cells isolated from IFN-γ–deficient (Ifnγ$^{-/-}$) mice. In contrast to reconstitution with WT CD8^{+} T cells that reduced the number of ILCs in the scWAT of Rag1$^{-/-}$ mice, reconstitution with Ifnγ$^{-/-}$ CD8^{+} T cells did not affect the number of ILCs in the scWAT of Rag1$^{-/-}$ mice (Supplemental Figure 5B). Additionally, reconstitution of Rag1$^{-/-}$ mice with CD8^{+} T cells derived from Ifnγ$^{-/-}$ mice did not alter the UCP1 expression in the scWAT, as opposed to its inhibition following reconstitution with WT CD8^{+} T cells (Figure 6, A and B), in further support of the contribution of IFN-γ in this process.

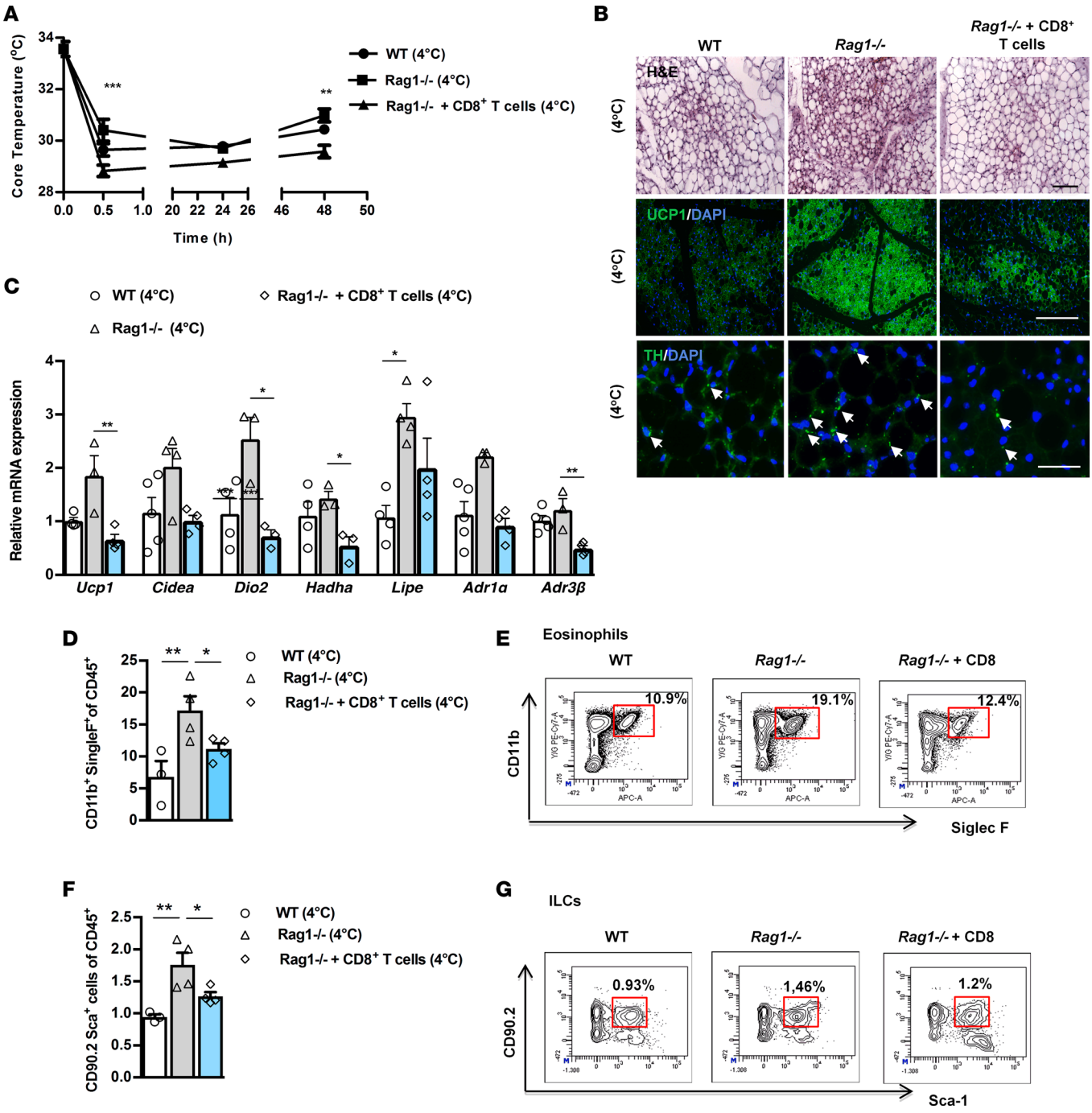

Figure 4. Adoptive transfer of CD8⁺ T cells inhibits increased scWAT beiging in Rag1$^{-/-}$ mice exposed to cold environment. Data shown are from the scWAT of WT, Rag1$^{-/-}$, or Rag1$^{-/-}$ mice reconstituted with 5×10^6 CD8⁺ T cells, once a week for 2 weeks. (**A**) Core temperature measurements. $n \geq 4$ per group. (**B**) Representative images of H&E and IF staining of UCP1 and TH. Arrows represent the TH⁺ cells. Scale bar: 100 μm. $n \geq 3$ per group. (**C**) Relative expression of thermogenic, lipid metabolism, and adrenergic receptors genes in the scWAT of age-matched mice, housed at 4°C for 2 days at the end of the second week. Data are shown as mean expression normalized to actin ± SEM. $n \geq 5$ per group. Data shown are derived from one representative of 2 independent experiments. (**D**) Representative percentages of eosinophils (CD11b⁺Siglec F⁺), housed at 4°C for 2 days. Data shown are representative of 2 independent experiments. Flow cytometry was performed after pooling $n \geq 4$ mice per group. (**E**) Results are expressed as percentages of CD11b⁺Siglec F⁺ eosinophils, gated on the viable CD45⁺DAPI⁻ cells. $n \geq 4$ per group. (**F**) Representative percentages of ILCs positive for CD90.2⁺ Sca-1⁺ Lin⁻ in WT mice or Rag1$^{-/-}$ mice treated with PBS or adoptively transferred with CD8⁺ T cells (5×10^6), once a week for 2 weeks, and housed at 4°C for 2 days are depicted on the flow cytometry plots. Data shown are representative of 2 independent experiments. Flow cytometry was performed after pooling $n \geq 4$ mice per group. (**G**) Results are expressed as percentages of CD90.2⁺Sca-1⁺ Lin⁻ gated on the viable CD45⁺DAPI⁻ cells. $n \geq 4$ per group. Data are presented as mean ± SEM. $^*P < 0.05$, $^{**}P < 0.01$, $^{***}P < 0.001$, 1-way ANOVA with Bonferroni's post test.

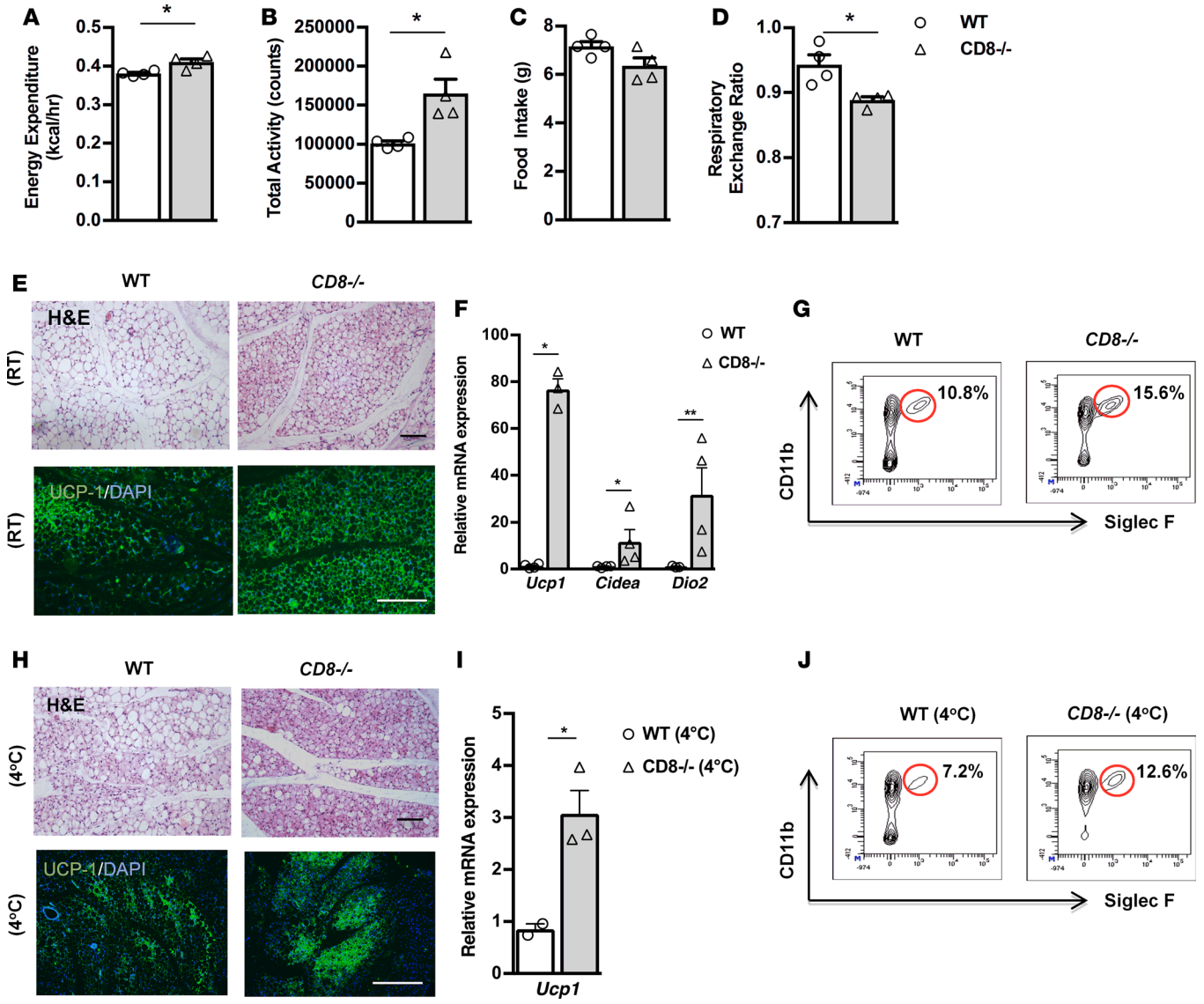

Figure 5. CD8$^{-/-}$ mice display increased beiging of scWAT and thermogenic capacity. (**A–D**) Assessment of metabolic behavior using indirect calorimetry, including energy expenditure adjusted to body weight (**A**), total activity (**B**), food intake (**C**), and respiratory exchange ratio (RER) (**D**). n = 4 per group. Data shown are derived from 1 experiment. (**E**) Representative H&E-stained images of scWAT of WT and CD8$^{-/-}$ mice. Scale bar: 100 μm. n = 3 per group. (**F**) Relative expression of beige genes, such as Ucp1, Cidea, and Dio2, in scWAT of CD8$^{-/-}$ mice versus WT mice. Data are shown as mean expression normalized to actin ± SEM. $n \geq 4$ per group. Data shown are derived from 1 representative of 2 independent experiments. (**G**) Single-cell suspensions prepared from scWAT, harvested from either WT or CD8$^{-/-}$ mice, were gated on the viable CD45^{+}DAPI^{-} cells and then depicted as percentages of Siglec F^{+} and CD11b^{+} cells to identify eosinophils. Flow cytometry was performed after pooling $n \geq 5$ mice per group. (**H**) Representative H&E-stained image of scWAT from WT and CD8$^{-/-}$ mice exposed to cold. Scale bar: 100 μm. n = 3 per group. (**I**) Relative expression of Ucp1 in scWAT from CD8$^{-/-}$ mice and WT mice. Data are shown as mean expression normalized to actin ± SEM. $n \geq 4$ per group. Data shown are derived from 1 experiment. (**J**) Single-cell suspensions from scWAT of WT and CD8$^{-/-}$ mice subjected to exposure at 4°C for 2 days were gated on the viable CD45^{+}DAPI^{-} cells and then analyzed for Siglec F and CD11b expression to measure eosinophils. Flow cytometry was performed after pooling $n \geq 5$ mice per group. Data are presented as mean ± SEM. $^{*}P < 0.05$, $^{**}P < 0.01$, Student's t test.

Next we sought to assess the importance of IFN-γ alone in beige adipogenesis by comparing the beiging of the scWAT in Ifn$\gamma^{-/-}$ and WT mice. In accordance with our previous findings, IFN-γ deficiency was associated with substantial expansion of the beige areas in the scWAT (Figure 6C), while there were no differences in the scWAT weights of the age- and weight-matched WT and Ifn$\gamma^{-/-}$ mice (Supplemental Figure 5C). Notably, the epiWAT weight of the Ifn$\gamma^{-/-}$ mice was significantly decreased compared with that of the WT epiWAT (Supplemental Figure 5C). Importantly, the Ifn$\gamma^{-/-}$ scWAT displayed increased numbers of eosinophils (Figure 6D) and of ILCs (Figure 6E) compared with WT scWAT, consistent with the mechanisms employed by CD8^{+} T cells to inhibit beige formation. Furthermore, a significant increase was noted

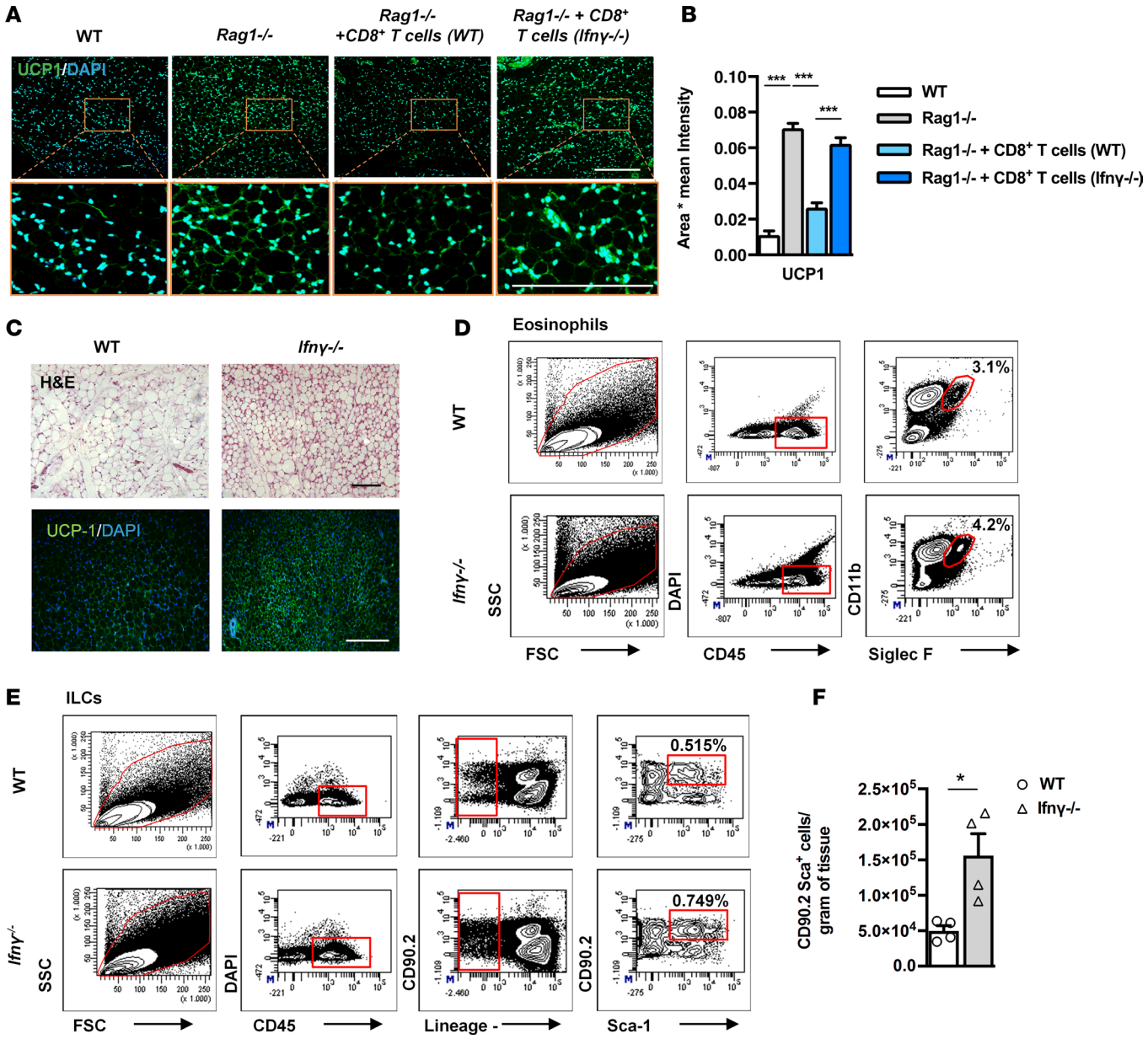

Figure 6. Increased beiging and eosinophils in the scWAT of Ifnγ$^{-/-}$ mice. (**A**) Representative images of UCP1 IF staining in the scWAT of WT or Rag1$^{-/-}$ mice treated with PBS or adoptively transferred with 5 × 10^6 WT-derived or Ifnγ$^{-/-}$-derived CD8$^+$ T cells, once a week for 2 weeks. Scale bar: 100 μm. (**B**) The relative UCP1 mean intensity in the above groups. Values represent mean ± SD intensity of 15 patches for every image. n = 3 per group. ***P < 0.001, 2-way ANOVA. (**C**) Representative images of H&E and UCP1 IF staining of scWAT from WT and Ifnγ$^{-/-}$ mice. Scale bar: 100 μm. n = 3 per group. Data shown are derived from 1 experiment. (**D**) Gating strategy for the identification of eosinophils gated on viable CD45$^+$DAPI$^-$ cells and further identified as CD11b$^+$Siglec F$^+$ cells. Data shown are depicted as percentages. Flow cytometry was performed after pooling n ≥ 4 mice per group. (**E**) Gating strategy for the identification of total ILCs in WT mice or Rag1$^{-/-}$ mice treated with PBS or adoptively transferred with 5 × 10^6 WT CD8$^+$ T cells or CD8$^+$ T cells derived from Ifnγ$^{-/-}$ mice, once a week for 2 weeks. Percentages of cells positive for CD90.2$^+$Sca-1$^+$Lin$^-$ gated on the viable CD45$^+$DAPI$^-$ cells are depicted on the flow cytometry plots. Flow cytometry was performed after pooling n ≥ 4 mice per group. (**F**) Absolute numbers of total ILCs (CD90.2$^+$ Sca-1$^+$Lin$^-$) per gram of tissue in scWAT of WT and Ifnγ$^{-/-}$ mice. n = 5 per group. Data are presented as mean ± SEM. *P < 0.05, Student's t test.

in the absolute numbers of eosinophils (WT: 810,000; Ifnγ$^{-/-}$: 1,100,000) and of ILCs per gram of tissue in Ifnγ$^{-/-}$ scWAT compared with WT scWAT (Figure 6F).

To summarize, our findings demonstrate that the inhibitory effects of CD8$^+$ T cells on the formation of beige fat are exerted at several levels, including regulation of the catecholaminergic input to the scWAT, targeting of specific adipocyte differentiation processes in an IFN-γ–dependent manner, and reduction of the abundance of cells of innate immunity (eosinophils, ILCs), and, thereby, a decrease of the levels of cytokines promoting beiging, such as IL-4, IL-5, and IL-13 (24) (Figure 7).

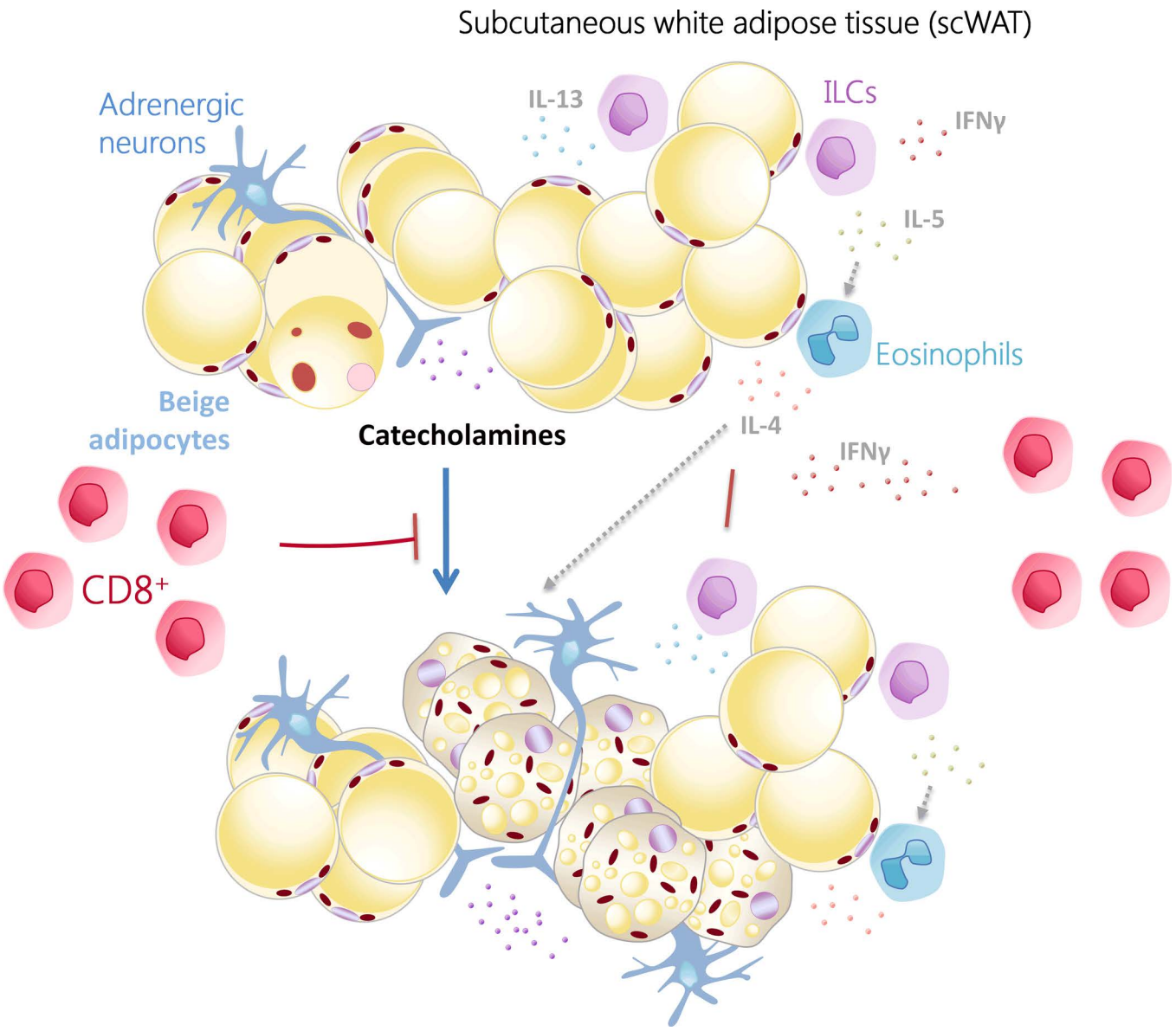

Figure 7. Schematic representation of the effects of the CD8⁺ T cells in the beiging of the scWAT. CD8⁺ T cells inhibit beige adipose tissue development in the scWAT by modulating the catecholaminergic input to scWAT and reducing the abundance of implicated innate immune cells and the associated cytokines, such as IL-4, IL-5, and IL-13, shown to induce beige fat formation (25). scWAT CD8⁺ T cells derived IFN-γ are a major mediator of these effects of the CD8⁺ T cells.

Discussion

In this paper, we describe a pathway in the regulation of beige adipogenesis, involving crosstalk of CD8⁺ T cells with catecholaminergic signaling and associated innate immune cells. In particular, we leveraged the Rag1$^{-/-}$ mouse model to unmask the significant contribution of T cells, particularly of CD8⁺ T cells, in energy homeostasis, as regulated at the level of the adipose tissue. We demonstrate that CD8⁺ T cell deficiency results in the induction of beige adipogenesis in the scWAT of Rag1$^{-/-}$ mice and corresponding changes in energy expenditure.

By employing several complementary approaches (CD8⁺ T cell reconstitution in Rag1-deficient, CD8⁺-deficient, or Ifn$\gamma^{-/-}$ mice), we can unequivocally demonstrate the inhibitory effect of CD8⁺ T cells on beige adipogenesis. Interestingly, we identified that several mechanisms involved in the immune plasticity and homeostatic functions of WAT likely cooperate with each other in mediating the inhibitory effect of CD8⁺ T cells on this process.

Our findings on increased expression in the scWAT of AdR(s) and TH, the rate-limiting enzyme for the synthesis of catecholamines, as well as drastic reduction of beiging upon treatment with the α-blocker prazosin hydrochloride, indicate the critical contribution of the increased catecholaminergic input in the beige adipogenesis in Rag1$^{-/-}$ mice. Although effects of α-adrenergic activation on lymphocytes have been reported (41–43), the potential effect of lymphopenia or lymphocytosis on catecholamine production and actions remains unknown (44). Notably, the catecholaminergic system in Rag1$^{-/-}$ mice retains its plasticity despite constitutive activation, as demonstrated by its sensitivity to temperature changes, including acclimatization or cold exposure, or even the reversal of catecholaminergic activity upon reconstitution of the missing CD8$^+$ T cells.

Interaction between adipocytes and cells of type 2 immunity was shown to regulate homeostasis and beige adipogenesis of the WAT in lean conditions. More specifically, it has been shown that beige fat development is dependent on ILC2s, eosinophils, and cytokines of type 2 immunity that act in concert to drive the differentiation of precursor cells to the smaller, multilocular beige adipocytes in specific WAT depots (24, 33). In agreement, Rag1$^{-/-}$ mice had increased ILCs in the scWAT that were dramatically decreased following reconstitution with CD8$^+$ T cells to levels resembling those in the WT tissue. We show that Rag1$^{-/-}$ mice, in addition to the increased ILCs and the associated cytokines, displayed increased IL-4 levels in the scWAT. On the other hand, both macrophage content and M2-specific markers were unaltered in the scWAT of Rag1$^{-/-}$ mice, suggesting that enhanced catecholaminergic signaling and beige adipogenesis in Rag1$^{-/-}$ mice do not necessarily involve alterations in macrophage numbers. These data indicate a CD8$^+$ T cell deficiency–mediated mechanism for beige adipogenesis that is not linked with alteration in M2 macrophage numbers, in further confirmation of the multifaceted regulation of this process (45). Reconstitution with CD8$^+$ T cells decreased the abundance of eosinophils and ILCs and blocked beige adipogenesis and the associated lipid oxidation in the scWAT of Rag1$^{-/-}$ mice, despite the deficiency in the other lymphocyte types. Furthermore, reversal of the Rag1$^{-/-}$ scWAT phenotype via replenishment of the missing CD8$^+$ T cells, led us to the hypothesis that CD8$^+$ T cells can counteract the effects of cells of innate immunity on beige adipogenesis. Our finding on increased beige adipogenesis in CD8$^{-/-}$ mice provided strong support for this hypothesis. Moreover, although this study has focused on the CD8$^+$ T cell–mediated regulation of beiging in the scWAT, the main fat depot with beiging capability, it is also conceivable that CD8$^+$ T cells might also act on other fat depots, such as epiWAT. Further, preliminary evidence from studies in CD4$^{-/-}$ mice suggested that CD4$^+$ T cells may also modulate beige adipogenesis, although in a less consistent manner, suggesting CD8$^+$ T cells as the predominant T cell group involved in beige adipogenesis. As the CD4$^+$ T cell pool is more diverse and more vulnerable to the experimental conditions applied, additional experiments are required to elucidate the exact positioning of this T cell subpopulation in the development of beige fat, which, however, needs to be addressed in a future study.

To further explore the mechanisms mediating the effects of CD8$^+$ T cells in beige adipogenesis, we assessed the effect of molecules secreted by CD8$^+$ T cells likely to effect on beige adipogenesis. According to the literature, obese Ifn$\gamma^{-/-}$ mice have been shown to have improved insulin sensitivity and decreased adipocyte size, suggesting the beneficial effects of IFN-γ deficiency for energy homeostasis (46). In line with this, we identified significant induction of beige fat generation and increased concentration of ILCs and eosinophils in the scWAT of Ifn$\gamma^{-/-}$ mice, all indicative of activation of mechanisms mediating utilization of energy. Finally, reconstitution of Rag1$^{-/-}$ mice with Ifn$\gamma^{-/-}$ CD8$^+$ T cells did not affect beige fat abundance in the scWAT, in contrast to the inhibitory (ablating) effect upon transfer of WT CD8$^+$ T cells. As established, CD8$^+$ T cells are not the only source of IFN-γ, as NK cells and ILC1 have been also shown as additional IFN-γ sources in the adipose tissue (47, 48). Assessment of the intra-scWAT levels of IFN-γ in Rag1$^{-/-}$ mice before and after reconstitution with CD8$^+$ T cells demonstrated that at least the contribution CD8$^+$ T cells to the total IFN-γ levels in this tissue is substantial (Supplemental Figure 5A) (49). Inhibition of beige adipogenesis upon reconstitution with CD8$^+$ T cells may be mediated by the increased intra-scWAT levels of IFN-γ, which might also exert dose-dependent effects on other inhibitors of beige adipogenesis. Notably, TH overexpression has been shown to decrease the production of IFN-γ (50), while challenge of PBMCs with IFN-γ decreased TH expression and the associated catecholamine production (43, 51). One other way to modulate IFN-γ levels and thus effect beige adipogenesis is to target upstream key pathways, such as IL-12 or STAT4 that lead to IFN-γ production or block IFN-γ itself (52). All of the above argue for operation of additional circuits among CD8$^+$ T cells, IFN-γ, and beige fat development.

Our findings raise the possibility for the potential benefits of targeted therapeutic interventions to leverage the effect of the $CD8^+$ T cells on the blockade of energy dissipation (15). Similar strategies targeting the inhibitory effect of $CD8^+$ T cells on the liver have been proposed for the treatment of diet-induced steatohepatitis and the associated hepatic carcinogenesis (32). Our findings also support the hypothesis that aggressive immunotherapies, for instance, employed in malignant and inflammatory disease, may substantially affect the regulation of energy homeostasis, which is already altered in these patients. This hypothesis raises the possibility that patients treated with immunomodulatory agents for cancer and other diseases may present with altered control of systemic metabolism, which, in a context-dependent manner, could also bear beneficial effects. Illuminating the specifics of the crosstalk between immunotherapeutic interventions and metabolism may provide a great benefit to patients, as these therapies extend to a number of diseases (14, 53, 54).

Methods

Animals and animal care. Age-matched (8–12 weeks) male mice, of $Rag1^{-/-}$, $CD8^{-/-}$, and IFN-$\gamma^{-/-}$ genotype, on C57BL/6J background were purchased from Jackson Laboratories and were bred in-house in a pathogen-free, temperature-controlled (22°C) environment, with a 12-hour-light/dark cycle, in accredited animal facilities at the Biomedical Research Foundation Academy Of Athens (BRFAA). Age- and weight-matched (22–25 g) WT mice with the above genotypes on C57BL/6J background were provided by the animal facilities at the BRFAA. All mice used for experimentation were provided by the colonies maintained in our facility for several generations in order to normalize facility-dependent changes in metabolic and other functions. Male mice 8–12 weeks of age were used at the start of each experiment. Mice were allocated randomly in experimental groups for each genotype.

Indirect calorimetry. Metabolic measurement was performed using an Oxymax indirect calorimetry system (Columbus Instruments). In short, preweighed mice were housed individually in specifically designed Oxymax calorimeter chambers with ad libitum access to diet and water for 72 hours, a 12-hour-light/dark cycle, and an ambient temperature of 22°C. Mice were singly housed for 2 days prior to transferring into the calorimeter chamber. VO_2, VCO_2, and rates were determined under Oxymax system settings as follows: air flow, 0.6 l/min; sample flow, 0.5 l/min. The system was calibrated against a standard gas mixture to measure O_2 consumed (VO_2, ml/kg/h) and CO_2 generated (VCO_2, ml/kg/h). Energy expenditure (kcal/h/kg), respiratory quotient (ratio of VCO_2/VO_2, RER), food intake (g), and activity (counts) were evaluated over a 48-hour period. The results were normalized and compared with the WT group per cohort, the results of which were set as 100%.

Tissue homogenization protocol for ELISA. scWAT from mice were weighed and homogenized with 600 μl cold HBSS (1×) supplemented with proteinase inhibitors (1:200) by using a tissue homogenizer. The homogenates were centrifuged at 400 *g* for 15 minutes at 4°C, and the supernatant was stored at –80C until analyzed. IL-4, IL-5, IL-13 (mouse IL-4, IL-5, IL-14 Elisa Ready-SET-Go!, eBioscience) and IFN-γ protein levels were determined by using ELISA (Biolegend ELISA Max).

Thermoneutrality experiment. Eight-week-old WT and $Rag1^{-/-}$ C57BL/6 mice were individually caged and housed at 28°C–30°C, with a 12-hour-light/dark cycle and free access to a standard chow diet for 20 days. Mice were housed in a controlled temperature room in the animal facilities at BRFAA.

Cold exposure experiment. Eight-week-old mice WT and $Rag1^{-/-}$ mice were housed in individual cages and acclimated at 18°C for 2 days followed by cold exposure at 4°C for another 2 days according to standard protocol. Core temperature was measured using an YSI Tele-Thermometer (Simpson Electric Co).

Histological analysis. Tissues were dissected, fixed in 4% paraformaldehyde solution overnight, and processed for routine paraffin histology. Paraffin-embedded tissues were sectioned at 5 μm and stained with H&E according to standard protocols. Adipocyte cell size was measured by automated software developed in our lab using Matlab. Images were obtained using a bright-field LEICA DMLS2 microscope. For immunohistochemistry, the tissues were incubated with 0.1% w/v Pronase (MilliporeSigma) at 37°C for 8 minutes and then washed again, blocked with PBS containing 10% normal goat serum and 0.1% Triton X-100 and incubated with the primary antibodies overnight at 4°C. UCP1 was detected using rabbit anti-Ucp1 antibody (ab10983, Abcam) at a concentration of 1:500, TH was detected by rabbit anti-TH (AB152; Millipore) at a concentration of 1:1,000, and β-tubulin was detected by mouse anti-Tuj1 (60052, STEMCELL Technologies Inc.). After several PBS washing steps, the tissue was incubated with the secondary antibody donkey anti-rabbit Alexa Fluor 488 (Thermo Fischer Scientific) or

donkey anti-mouse Alexa Fluor 568 (Thermo Fischer Scientific). Another washing step was followed by DAPI incubation and further washing steps before the sections were mounted using Vectashield mounting medium (Vector). For quantification of TH expression, parenchymal nerve fibers (Tuj1$^+$) were measured in 5 randomly selected area of the depot. Images were obtained using a confocal inverted LEICA TCS SP5 (DMI6000). For UCP1 quantification, patches (15 patches for every image, sized 128 × 128 pixels) of images were randomly selected, and the mean intensity of the staining was measured.

Adoptive transfer studies. To examine the effects of T cells in beige adipogenesis, 12-week-old Rag1$^{-/-}$ mice fed a chow diet were used for adoptive transfer of splenocytes, cells rich in B and T cells. Additionally, Rag1$^{-/-}$ mice, kept either at 24°C or 4°C, were adoptively transferred with CD8$^+$ T cells. Splenocytes were obtained from the spleens of lean C57BL/6 WT mice and dissociated into single-cell suspensions and red blood cells were removed. CD8$^+$ T cells were purified from the spleens of WT C57BL/6 male mice using mouse CD8α (Ly-2) microbeads (130-049-401, Miltenyi Biotec) according to the manufacturer's protocol. A total of 5 × 10^6 splenocytes containing 15%–20% CD8$^+$ T cells (around 8 × 10^5) or 5 × 10^6 CD8$^+$ T cells were injected retro-orbitally weekly and sacrificed after 2 weeks. Control groups received retro-orbital injections of PBS. Purity of CD8$^+$ T cells injected was measured by FACS analysis and was >85%. Homing of CD8$^+$ T cells in the scWAT was confirmed by flow cytometry analysis.

In vivo depletion of CD8$^+$ T cells. WT mice received 200 μg anti-CD8 antibody (BE0004-1, Bio X Cell) or normal rat IgG (control) (Bio X Cell) by the i.p. route at days 0, 2, and 6. Mice were euthanized at day 10 for further analysis. The depletion was assessed at days 24 hours after the treatment with mAbs by flow cytometric blood analysis.

scWAT preparation for flow cytometry analysis. scWAT was removed, weighed after careful removal of lymph nodes, and kept on ice in 3-cm dishes with Buffer I (PBS with 1 mM $CaCl_2$ and 0.5% BSA). The tissue was finely minced and washed with Buffer I at 500 *g* at 4°C for 10 minutes to remove erythrocytes and free leukocytes. The floating tissue (upper phase) was removed following centrifugation and was further dispersed by shaking into DMEM (high glucose) medium containing fresh collagenase D (2mg/ml) and 0.5% BSA (1 ml/ tissue g) at 37°C for 30–40 minutes with gentle agitation. Cell suspension was topped up to 10 ml by DMEM medium and then passed through 100-μm filters to generate single-cell suspensions, before being centrifuged at 300 *g* for 5 minutes to separate floating adipocytes from the SVF pellet. The cell pellet was resuspended in FACS buffer (PBS with 0.1% BSA and 2.5 mM EDTA) prior to staining with the indicated antibodies.

Flow cytometry. scWAT was processed and stained with fluorochrome-conjugated monoclonal antibody combinations for ILC staining. Monoclonal antibodies used for flow cytometry were as follows: allophycocyanin (APC) anti-CD45 (30-F11; Biolegend); phycoerythrin (PE) anti-CD3 (145-2C11; Biolegend); PE anti-CD4 (E121.19; Biolegend); PE anti-CD8 (53-6.7; Biolegend); PE anti-CD19 (6D5; Biolegend); PE anti-B220 (RA3-6B2; Biolegend); FITC CD11b (M1/70; Biolegend); PE anti-CD11c (N418; Biolegend); PE anti-FceRI (MAR-1; Biolegend); PE anti-Gr-1 (RB6-8C5; Biolegend); PE anti-Ter119 (Ter/119; Biolegend); peridinin-chlorophyll proteins (PercP) anti-CD90.2 (53-2.1; Biolegend); PE/Cy7 anti-Sca1 (D7; Biolegend) and Alexa Fluor 488–Gata3 (16E10A23; Biolegend). Representative gating schemes for each population are shown in Figure 3D. ILCs are identified as CD45$^+$, lineage$^-$ (CD3$^-$CD4$^-$CD8$^-$CD19$^-$B220$^-$CD11b$^-$CD11c$^-$FceRI$^-$Gr-1$^-$Terr119$^-$) CD90.2$^+$ Sca-1$^+$ cells. scWATs were processed and stained with fluorochrome-conjugated monoclonal antibody combinations for eosinophil staining. Eosinophils were identified as CD45$^+$, CD11b$^+$, and Siglec F$^+$ cells. Representative gating schemes are shown in Figure 3F. Trafficking of CD45$^+$CD3$^+$CD8$^+$ in the scWAT was assessed using the following monoclonal antibodies: APC anti-CD45 (30-F11; Biolegend); FITC anti-CD3 (145-2C11; Biolegend), and PeCy7 anti-CD8 (53-6.7; Biolegend). Representative gating schemes are shown in Supplemental Figure 2A. Macrophage assessment of the subcutaneous adipose tissue was assessed by staining with the following fluorochrome-conjugated monoclonal antibodies: APC anti-CD45 (30-F11; Biolegend); FITC anti-CD11b$^+$ (M1/70; Biolegend); and PE F480$^+$ (BM8; eBioscience). Representative gating schemes are shown in Supplemental Figure 2B. Samples were analyzed on a FACSAria III (Becton Dickinson). As indicated, data are expressed as percentages of CD45$^+$ hematopoietic cells. Live lymphocytes were gated by DAPI exclusion, size, and granularity based on forward- and side-scatter. Data were analyzed using BD FACSDiVa software. Appropriate isotype-matched controls for all antibodies were used to determine positive staining.

Western blot. Tissues were harvested in RIPA buffer (ThermoFisher Scientific) with 1% protease and 1% phosphatase inhibitors (ThermoFisher Scientific). 20 ng protein was loaded into each well of a 4%–12% Bis-Tris polyacrylamide gel (ThermoFischer Scientific) and transferred to nitrocellulose membrane (ThermoFischer Scientific). Protein-bound membranes were blocked for 30 minutes with 5% nonfat dry milk in 0.1% Tris-buffered saline with Tween and incubated with rabbit anti-Ucp1 antibody (ab10983, Abcam) or anti-tubulin (ab15568, Abcam) in blocking buffer overnight at 4°C. Membranes were treated with HRP-conjugated secondary antibodies diluted 1:5,000 in blocking buffer for 2 hours and rinsed with Pierce ECL chemiluminescent solution (Thermo Fischer Scientific). Membranes were immediately read in a Kodak Image Station 4000 mm PRO, and protein levels were quantified using ImageJ (NIH) free, open-source software.

Quantitative real-time RT-PCR. Total RNA was isolated from tissues using TRI reagent (MilliporeSigma) and treated with DNase using the DNA-free kit (Ambion). Complementary DNA was made from 2 μg total RNA by MMLV reverse transcriptase (Invitrogen) and initiated from random hexamer primers (Life Technologies Inc). Quantitative real-time PCR analysis was performed using RT² SYBR Green qPCR Master Mix (SA biosciences) in a ABI PRISM 7000 Sequence Detection System (Applied Biosystems). Primers used for real-time PCR are shown in Supplemental Table 1. Gene expression levels were normalized to actin in vivo and calculated according to the $2^{-\Delta\Delta Ct}$ method.

Adrenergic blockade. For α-adrenergic blockade, prazosin hydrochloride (MilliporeSigma), a selective α1-adrenergic antagonist, was administered via the drinking water (8 mg/kg) for 5 days.

Statistics. Data are presented as mean ± SEM. All statistical analysis was performed using GraphPad Prism software version 5.0. The statistical significance of the differences between various treatments was measured by either the 2-tailed Student's *t* test or 1-way ANOVA with Bonferroni's post-test. A *P* value of less than 0.05 was considered statistically significant. Sample size, number of replicates, and statistical tests are reported in figure legends.

Study approval. All experimental procedures reported here were approved by the competent veterinary authority of the prefectures of Athens, Greece, in accordance with the National Registration (Presidential Decree 56/2013) and with European Directive 63/2010.

Author contributions

MM, SK, EK, YK, and KK designed and performed experiments and analyzed and interpreted the data. SO and AK were involved with some of the in vivo experiments. PT analyzed data. MS and EA designed and performed flow cytometry studies and provided the Ifnγ-knockout mice. NK is the veterinarian and reviewed all experimental protocols and supervised all animal studies. AC, SK, KJC, DS, SB, MWS, and TC were involved in experimental design and data interpretation. TC was involved in editing of the manuscript. KPK planned and designed the experiments; supervised all experiments and interpretation of results with SK; coordinated the writing of the manuscript by SK, MM, and EK; and edited the final manuscript.

Acknowledgments

This work was supported by the European Union 7th Framework Programme, Regpot activity grant 245928 (TRANSMED), and Cooperation Programme 305739 (RISKYCAD), and Greek national funds through the Operational Program "Education and Lifelong Learning" of the National Strategic Reference Framework–Research Funding Program: Herakletus II. This work was cofinanced by the European Union (European Social Fund). SK was funded by NIH grant R21EB019079, the National Strategic Reference Framework 2007-2013 Programme for Development (EU Regional Development Fund), and the Greek Ministry of Education and Religious Affairs, Culture & Sports.

Address correspondence to: Katia Karalis, Emulate Inc., 27 Drydock Ave., Boston, Massachusetts 02210, USA. Phone: 508.843.5324; Email: katia.karalis@childrens.harvard.edu or katia.karalis@eulatebio.com. Or to: Sevasti Karaliota, Biomedical Research Foundation Academy of Athens, Soranou Efesiou 4, Athens 11527, Greece. Phone: 30.2106597240; Email: skaral@bioacademy.gr.

KPK's present address is: Emulate Inc., Boston, Massachusetts, USA.

1. Lumeng CN, Bodzin JL, Saltiel AR. Obesity induces a phenotypic switch in adipose tissue macrophage polarization. *J Clin Invest*. 2007;117(1):175–184.
2. Shi MA, Shi GP. Different roles of mast cells in obesity and diabetes: lessons from experimental animals and humans. *Front Immunol*. 2012;3:7.
3. Wu D, et al. Eosinophils sustain adipose alternatively activated macrophages associated with glucose homeostasis. *Science*. 2011;332(6026):243–247.
4. Talukdar S, et al. Neutrophils mediate insulin resistance in mice fed a high-fat diet through secreted elastase. *Nat Med*. 2012;18(9):1407–1412.
5. Molofsky AB, et al. Innate lymphoid type 2 cells sustain visceral adipose tissue eosinophils and alternatively activated macrophages. *J Exp Med*. 2013;210(3):535–549.
6. Winer S, et al. Normalization of obesity-associated insulin resistance through immunotherapy. *Nat Med*. 2009;15(8):921–929.
7. Nishimura S, et al. CD8+ effector T cells contribute to macrophage recruitment and adipose tissue inflammation in obesity. *Nat Med*. 2009;15(8):914–920.
8. Feuerer M, et al. Lean, but not obese, fat is enriched for a unique population of regulatory T cells that affect metabolic parameters. *Nat Med*. 2009;15(8):930–939.
9. Cipolletta D, et al. PPAR-γ is a major driver of the accumulation and phenotype of adipose tissue Treg cells. *Nature*. 2012;486(7404):549–553.
10. Scherer PE. Adipose tissue: from lipid storage compartment to endocrine organ. *Diabetes*. 2006;55(6):1537–1545.
11. Vosselman MJ, van Marken Lichtenbelt WD, Schrauwen P. Energy dissipation in brown adipose tissue: from mice to men. *Mol Cell Endocrinol*. 2013;379(1-2):43–50.
12. Fedorenko A, Lishko PV, Kirichok Y. Mechanism of fatty-acid-dependent UCP1 uncoupling in brown fat mitochondria. *Cell*. 2012;151(2):400–413.
13. Cohen P, et al. Ablation of PRDM16 and beige adipose causes metabolic dysfunction and a subcutaneous to visceral fat switch. *Cell*. 2014;156(1-2):304–316.
14. Ishibashi J, Seale P. Medicine. Beige can be slimming. *Science*. 2010;328(5982):1113–1114.
15. Harms M, Seale P. Brown and beige fat: development, function and therapeutic potential. *Nat Med*. 2013;19(10):1252–1263.
16. Wu J, et al. Beige adipocytes are a distinct type of thermogenic fat cell in mouse and human. *Cell*. 2012;150(2):366–376.
17. Lee YH, Petkova AP, Mottillo EP, Granneman JG. In vivo identification of bipotential adipocyte progenitors recruited by β3-adrenoceptor activation and high-fat feeding. *Cell Metab*. 2012;15(4):480–491.
18. Petrovic N, Walden TB, Shabalina IG, Timmons JA, Cannon B, Nedergaard J. Chronic peroxisome proliferator-activated receptor gamma (PPARgamma) activation of epididymally derived white adipocyte cultures reveals a population of thermogenically competent, UCP1-containing adipocytes molecularly distinct from classic brown adipocytes. *J Biol Chem*. 2010;285(10):7153–7164.
19. Schulz TJ, et al. Brown-fat paucity due to impaired BMP signalling induces compensatory browning of white fat. *Nature*. 2013;495(7441):379–383.
20. Shabalina IG, Petrovic N, de Jong JM, Kalinovich AV, Cannon B, Nedergaard J. UCP1 in brite/beige adipose tissue mitochondria is functionally thermogenic. *Cell Rep*. 2013;5(5):1196–1203.
21. Boström P, et al. A PGC1-α-dependent myokine that drives brown-fat-like development of white fat and thermogenesis. *Nature*. 2012;481(7382):463–468.
22. Qiu Y, et al. Eosinophils and type 2 cytokine signaling in macrophages orchestrate development of functional beige fat. *Cell*. 2014;157(6):1292–1308.
23. Ye L, et al. Fat cells directly sense temperature to activate thermogenesis. *Proc Natl Acad Sci USA*. 2013;110(30):12480–12485.
24. Lee MW, et al. Activated type 2 innate lymphoid cells regulate beige fat biogenesis. *Cell*. 2015;160(1-2):74–87.
25. Chung KJ, et al. A self-sustained loop of inflammation-driven inhibition of beige adipogenesis in obesity. *Nat Immunol*. 2017;18(6):654–664.
26. Shan B, et al. The metabolic ER stress sensor IRE1α suppresses alternative activation of macrophages and impairs energy expenditure in obesity. *Nat Immunol*. 2017;18(5):519–529.
27. Seale P, et al. Prdm16 determines the thermogenic program of subcutaneous white adipose tissue in mice. *J Clin Invest*. 2011;121(1):96–105.
28. Feldmann HM, Golozoubova V, Cannon B, Nedergaard J. UCP1 ablation induces obesity and abolishes diet-induced thermogenesis in mice exempt from thermal stress by living at thermoneutrality. *Cell Metab*. 2009;9(2):203–209.
29. Cui X, et al. Thermoneutrality decreases thermogenic program and promotes adiposity in high-fat diet-fed mice. *Physiol Rep*. 2016;4(10):e12799.
30. Gospodarska E, Nowialis P, Kozak LP. Mitochondrial turnover: a phenotype distinguishing brown adipocytes from interscapular brown adipose tissue and white adipose tissue. *J Biol Chem*. 2015;290(13):8243–8255.
31. Mathis D. Immunological goings-on in visceral adipose tissue. *Cell Metab*. 2013;17(6):851–859.
32. Wolf MJ, et al. Metabolic activation of intrahepatic CD8+ T cells and NKT cells causes nonalcoholic steatohepatitis and liver cancer via cross-talk with hepatocytes. *Cancer Cell*. 2014;26(4):549–564.
33. Brestoff JR, et al. Group 2 innate lymphoid cells promote beiging of white adipose tissue and limit obesity. *Nature*. 2015;519(7542):242–246.
34. Lee MW, et al. Activated type 2 innate lymphoid cells regulate beige fat biogenesis. *Cell*. 2015;160(1-2):74–87.
35. Nguyen KD, et al. Alternatively activated macrophages produce catecholamines to sustain adaptive thermogenesis. *Nature*. 2011;480(7375):104–108.
36. Nedergaard J, Cannon B. UCP1 mRNA does not produce heat. *Biochim Biophys Acta*. 2013;1831(5):943–949.
37. Thomas SA, Palmiter RD. Thermoregulatory and metabolic phenotypes of mice lacking noradrenaline and adrenaline. *Nature*. 1997;387(6628):94–97.
38. Zhou QY, Quaife CJ, Palmiter RD. Targeted disruption of the tyrosine hydroxylase gene reveals that catecholamines are required for mouse fetal development. *Nature*. 1995;374(6523):640–643.
39. Huh JY, Park YJ, Ham M, Kim JB. Crosstalk between adipocytes and immune cells in adipose tissue inflammation and meta-

bolic dysregulation in obesity. *Mol Cells*. 2014;37(5):365–371.
40. Huh JY, Park YJ, Ham M, Kim JB. Crosstalk between adipocytes and immune cells in adipose tissue inflammation and metabolic dysregulation in obesity. *Mol Cells*. 2014;37(5):365–371.
41. Pesić V, et al. Expression of alpha1-adrenoceptors on thymic cells and their role in fine tuning of thymopoiesis. *J Neuroimmunol*. 2009;214(1-2):55–66.
42. Krüger K, Lechtermann A, Fobker M, Völker K, Mooren FC. Exercise-induced redistribution of T lymphocytes is regulated by adrenergic mechanisms. *Brain Behav Immun*. 2008;22(3):324–338.
43. Qiu YH, Cheng C, Dai L, Peng YP. Effect of endogenous catecholamines in lymphocytes on lymphocyte function. *J Neuroimmunol*. 2005;167(1-2):45–52.
44. Wolf Y, et al. Brown-adipose-tissue macrophages control tissue innervation and homeostatic energy expenditure. *Nat Immunol*. 2017;18(6):665–674.
45. Fischer K, et al. Alternatively activated macrophages do not synthesize catecholamines or contribute to adipose tissue adaptive thermogenesis. *Nat Med*. 2017;23(5):623–630.
46. O'Rourke RW, et al. Systemic inflammation and insulin sensitivity in obese IFN-γ knockout mice. *Metab Clin Exp*. 2012;61(8):1152–1161.
47. Arase H, Arase N, Saito T. Interferon gamma production by natural killer (NK) cells and NK1.1+ T cells upon NKR-P1 cross-linking. *J Exp Med*. 1996;183(5):2391–2396.
48. Jiao Y, Huntington ND, Belz GT, Seillet C. Type 1 innate lymphoid cell biology: Lessons learnt from natural killer cells. *Front Immunol*. 2016;7:426.
49. Vielma SA, Klein RL, Levingston CA, Young MR. Adipocytes as immune regulatory cells. *Int Immunopharmacol*. 2013;16(2):224–231.
50. Huang HW, Zuo C, Chen X, Peng YP, Qiu YH. Effect of tyrosine hydroxylase overexpression in lymphocytes on the differentiation and function of T helper cells. *Int J Mol Med*. 2016;38(2):635–642.
51. Cosentino M, et al. Interferon-gamma and interferon-beta affect endogenous catecholamines in human peripheral blood mononuclear cells: implications for multiple sclerosis. *J Neuroimmunol*. 2005;162(1-2):112–121.
52. Lund RJ, Chen Z, Scheinin J, Lahesmaa R. Early target genes of IL-12 and STAT4 signaling in th cells. *J Immunol*. 2004;172(11):6775–6782.
53. McPhee JB, Schertzer JD. Immunometabolism of obesity and diabetes: microbiota link compartmentalized immunity in the gut to metabolic tissue inflammation. *Clin Sci*. 2015;129(12):1083–1096.
54. Jones L, et al. Genetic evidence implicates the immune system and cholesterol metabolism in the aetiology of Alzheimer's disease. *PLoS One*. 2010;5(11):e13950.